Atlantic Tropical Cyclone Monitoring with AMSU-A: Estimation of Maximum Sustained Wind Speeds

ROY W. SPENCER

NASA Marshall Space Flight Center, Global Hydrology and Climate Center, Huntsville, Alabama

WILLIAM D. BRASWELL

Computer Sciences Corporation, Global Hydrology and Climate Center, Huntsville, Alabama

(Manuscript received 6 May 2000, in final form 17 October 2000)

ABSTRACT

The first Advanced Microwave Sounding Unit temperature sounder (AMSU-A) was launched on the *NOAA-15* satellite on 13 May 1998. The AMSU-A's higher spatial and radiometric resolutions provide more useful information on the strength of the middle- and upper-tropospheric warm cores associated with tropical cyclones than have previous microwave temperature sounders. The gradient wind relationship suggests that the temperature gradient near the core of tropical cyclones increases nonlinearly with wind speed. The gradient wind equation is recast to include AMSU-A-derived variables. Stepwise regression is used to determine which of these variables is most closely related to maximum sustained winds (V_{max}). The satellite variables investigated include the radially averaged gradients at two spatial resolutions of AMSU-A channels 1–10 T_b data ($\delta_r T_b$), the squares of these gradients, a channel-15-based scattering index (SI_{89}), and area-averaged T_b. Calculations of T_b and $\delta_r T_b$ from mesoscale model simulations of Andrew (1992) reveal the effects of the AMSU spatial sampling on the cyclone warm core presentation. Stepwise regression of 66 AMSU-A terms against National Hurricane Center V_{max} estimates from the 1998 and 1999 Atlantic hurricane season confirms the existence of a nonlinear relationship between wind speed and radially averaged temperature gradients near the cyclone warm core. Of six regression terms, four are dominated by temperature information, and two are interpreted as correcting for hydrometeor contamination. Jackknifed regressions were performed to estimate the algorithm performance on independent data. For the 82 cases that had in situ measurements of V_{max}, the average error standard deviation was 4.7 m s^{-1}. For 108 cases without in situ wind data, the average error standard deviation was 7.5 m s^{-1}. Operational considerations, including the detection of weak cyclones and false alarm reduction, are also discussed.

1. Introduction

The potential for monitoring of tropical cyclone strength with satellite-based passive microwave temperature sounders has been known for over 20 years (Kidder et al. 1978; Grody et al. 1979). Previous investigations have utilized the Scanning Microwave Spectrometer (SCAMS; Kidder et al. 1978, 1980) or microwave sounding units (MSU; Velden and Smith 1983; Velden 1989; Velden et al. 1991) to quantitatively diagnose central pressure, radius of 15 and 25 m s^{-1} winds, or maximum sustained wind speed (V_{max}) in mature tropical cyclones. These techniques have considerable physical basis through hydrostatic and gradient wind relationships. Past sounders have had rather poor spatial resolution (110 km at best), limiting their utility in discerning the upper-tropospheric temperature gradients associated with the cores of tropical cyclones from the brightness temperatures (T_b) observed by the sounders. With the May 1998 launch of the first Advanced Microwave Sounding Unit (AMSU-A) on the *15th National Oceanic and Atmospheric Administration* (*NOAA-15*) satellite, 50-km spatial resolution is now available with relatively low radiometric noise (0.15°C). While this resolution is still not sufficient to fully the resolve the warm core of most tropical cyclones, we will show it is sufficient to provide useful information on V_{max}.

In the previous studies, the warmest upper-tropospheric brightness temperature T_b measurement (or retrieved 250-hPa temperature) near the storm center was differenced with some measure of the environmental temperature, usually at a distance of several hundred kilometers from the warm core. This estimate of warmth was then quantitatively related to the minimum sea level pressure in the storm, maximum sustained wind speed, or the radially averaged wind field. While we will re-

Corresponding author address: Roy W. Spencer, NASA Marshall Space Flight Center, Global Hydrology and Climate Center, 320 Sparkman Drive, Huntsville, AL 35805.
E-mail: Roy.Spencer@msfc.nasa.gov

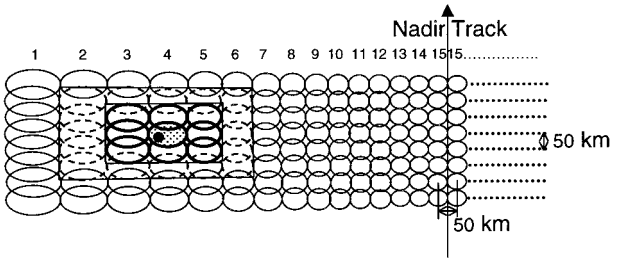

FIG. 1. AMSU-A sampling geometry, including the hypothetical location of the center of circulation of a tropical cyclone (dot), and the inner and outer footprint grids for which radially averaged brightness temperature gradients are computed.

strict our analysis of AMSU-A data to only the diagnosis of the cyclone maximum sustained wind, the AMSU-A data could also support estimates of minimum central pressure and the spatial extent of the cyclone wind field. The estimation of minimum sea level pressure in the storm might be considered an easier quantity to estimate since the spatial extent of the eye is typically larger than the region of maximum temperature gradient that lies above the region of maximum sustained winds, and so would be more consistent with the AMSU spatial resolution.

Our study builds upon the previous efforts in several ways. Foremost is the availability of AMSU-A data for the 1998 and 1999 hurricane seasons (our archive begins 3 Aug 1998). Second, instead of addressing only mature hurricanes, we examine all storms, depression through hurricane strength, reported by the National Hurricane Center in their ''best track'' (Jarvinen et al. 1984) archive for the 1998 and 1999 seasons. This allows some insight into the ability of AMSU-A to monitor prehurricane disturbances. Third, in contrast to previous studies, we will use most of the swath width of the AMSU, rather than restricting the analysis to only those storms that happen to be near the center of the satellite data swath. This increases the potential of the technique in an operational environment. Fourth, we address the sensitivity of the AMSU-A sounding channels to hydrometeor contamination.

We provide an updated theoretical basis for the relationship between $V_{\max}$ and radially averaged deep layer temperature gradients centered on the cyclone warm core. This updated analysis guided our choice of variables for the regression analysis. We also illustrate some of the AMSU spatial sampling effects with mesoscale model simulations of Hurricane Andrew (1992).

2. The AMSU instrument and limb corrections

a. Instrument characteristics

The AMSU-A is a 15-channel temperature sounder operating at frequencies from 23.8 to 89.0 GHz. The AMSU-A unit has three separate antenna systems designed to provide nearly the same spatial resolution (50 km, as opposed to 110 km for the MSU) at all frequencies. It scans cross-track and samples 30 footprints (as opposed to the MSUs' 11) from 48⅓° left of nadir to 48⅓° right of nadir in steps of 3⅓° (see Fig. 1). With a scan period of 8 s and a *NOAA-15* ground track speed of about 6.7 km s^{-1}, successive scan lines are separated by about 50 km (in contrast to 150 km for the MSU). The AMSU-A has the radiometric characteristics listed in Table 1.

TABLE 1. AMSU-A radiometer characteristics. Channels with the greatest sensitivity to hurricane warm cores are in bold type. Those channels with the greatest sensitivity to liquid or ice hydrometeors are in bold italics. The temperature sensitivities (noise values) are averages of AeroJet measured values of the first three flight models of the instrument.

Channel no.	Frequency (GHz)	Noise (measured, °C)	Weighting function peak
1	***23.8***	***0.17***	***Surface***
2	***31.4***	***0.23***	***Surface***
3	***50.3***	***0.25***	***Surface***
4	52.8	0.15	900 hPa
5	53.596	0.15	600 hPa
6	**54.4**	**0.14**	**400 hPa**
7	**54.94**	**0.14**	**250 hPa**
8	**55.5**	**0.15**	**150 hPa**
9	$\nu_1 = 57.290344$	0.17	90 hPa
10	$\nu_1 \pm 0.217$	0.22	50 hPa
11	$\nu_1 \pm 0.3222 \pm 0.048$	0.24	25 hPa
12	$\nu_1 \pm 0.3222 \pm 0.022$	0.36	10 hPa
13	$\nu_1 \pm 0.3222 \pm 0.010$	0.48	5 hPa
14	$\nu_1 \pm 0.3222 \pm 0.0045$	0.80	2.5 hPa
15	***89.0***	***0.15***	***Surface***

b. The T_b calibration and limb correction

We calibrated the data following the method described by Mo (1996), utilizing the calibration coefficients contained in the Level 1b orbit files, and then converted the resulting radiances to T_b by inverting the Planck equation. The T_b were then limb corrected with a procedure described in the appendix. Hereafter, limb-corrected T_b for channel i will be designated T_{bi} and AMSU-A will be referred to as simply AMSU.

While pressure level temperatures can be retrieved from the AMSU measurements, such procedures require that assumptions be made about the data. We choose not to bias the temperature information by additional assumptions and to work directly with the sounder measurements. This also simplifies the data processing in the operational application of the method.

3. Theory

a. Basis for the method

As pointed out by Kidder et al. (1980), the gradient wind relationship is a good approximation for tropical cyclone winds at the gradient wind level. It is written as

$$\frac{V_g^2}{R} + fV_g = -\frac{d\Phi}{dn}, \tag{1}$$

where V_g is wind speed at a gradient wind level, R is the radius of curvature of the flow, f is the Coriolis parameter, Φ is the geopotential height, and n is the radial flow. Equation (1) can be rearranged to give

$$V_g = -\frac{fR}{2} \pm \sqrt{\frac{f^2R^2}{4} - R\frac{d\Phi}{dn}}, \tag{2}$$

where the positive root applies to cyclonic flow. The geopotential height is conventionally defined as

$$\Phi(z) = \int_{\text{surface}}^{z} g\, dz. \tag{3}$$

We find, however, that an alternative definition of geopotential height, using a reference level in the stratosphere, provides a more straightforward conceptual framework for interpreting satellite deep layer temperature measurements of cyclones (Spencer et al. 1995). Since the geopotential so referenced is not really a height, but rather a thickness, we will use the symbol Ψ to represent it. For this upper reference level we use the level of insignificant dynamics (LID) introduced by Hirschberg and Fritsch (1993). They provide strong justification for ''the existence of a stratospheric level of insignificant dynamics (LID) where the height (pressure) tendency may be considered negligible on the scale of cyclones.'' For our work, this cyclone scale height invariant pressure surface (the LID) is assumed to exist and, as stated, we use it as the reference surface for the geopotential. We define the geopotential thickness, referenced to the LID, as

$$\Psi(z) = \int_{z}^{\text{LID}} g\, dz. \tag{4}$$

Now since

$$\frac{d\Psi}{dn} = -\frac{d\Phi}{dn}$$

and choosing the cyclonic flow root, Eq. (2) becomes

$$V_g = -\frac{fR}{2} + \sqrt{\frac{f^2R^2}{4} + R\frac{d\Psi}{dn}}. \tag{5}$$

In this equation the primary dynamical variable upon which wind speed depends is the geopotential thickness Ψ. We find empirically that brightness temperature gradients from the AMSU sounding channels near the tropical cyclone center are closely related to maximum sustained wind speeds at the surface. The maximum surface winds are usually estimated from hurricane reconnaissance flight-level winds extrapolated down to the surface or from dropwindsondes (Franklin et al. 2000). This observed empirical relationship between brightness temperature and wind speed can be explained conceptually by invoking the LID assumption. In the remainder of this section we show the theoretical basis for this relationship. We proceed based on four primary assumptions. They are 1) the existence of a cyclone scale LID, 2) hydrostatics is valid on cyclone scales (Kidder et al. 1978, 1980), 3) the surface emission makes negligible contributions to the brightness temperature (for the microwave channels we use), and 4) the temperature profile, T, in a cyclone can be represented by $T(r, z) = T_e + \alpha(r)\hat{T}(z)$, where T_e is the environmental temperature just external to the storm, α is a scaling factor dependent only on the radial distance from the center of the storm, and $\hat{T}$ is a standard anomaly profile with constant shape for all storms. The functional form of α can vary from storm to storm. Kidder et al. (1980) also used this assumption of an anomaly profile with invariant shape. It is supported by temperature anomaly measurements from West Pacific typhoons and Atlantic (West Indies) hurricanes (Nunez and Gray 1977).

With negligible contributions from surface emission, the brightness temperature T_b is defined as

$$T_b = \int_{P_{\text{bottom}}}^{P_{\text{top}}} WT\, d\, \ln P, \tag{6}$$

where the bounds on the integral are such that the weighting function is negligible above the upper bound and below the lower bound. The very slight dependence of the microwave weighting functions on temperature is neglected. Assuming T in a storm can be approximated as $T(r, z) = T_e + \alpha(r)\hat{T}(z)$, Eq. (6) becomes

$$\begin{aligned} T_b &= \int_{P_{\text{bottom}}}^{P_{\text{top}}} W(T_e + \alpha T)\, d\, \ln P \\ &= T_{be} + \alpha \int_{P_{\text{bottom}}}^{P_{\text{top}}} W\hat{T} d\, \ln P, \end{aligned} \tag{7}$$

where T_{be} is the brightness temperature of a profile in the surrounding environment.

Assuming the validity of hydrostatics and the ideal gas law, we have

$$\frac{dP}{dz} = -\rho g = -\frac{Pg}{R_g T}, \tag{8}$$

where R_g is the ideal gas constant and ρ is the density. Rearranging and integrating from P to the LID gives

$$\Psi(P) = \int_{P}^{\text{LID}} g\, dz = -R_g \int_{P}^{\text{LID}} T\, d\, \ln P, \tag{9}$$

where the definition of geopotential was also invoked. Again invoking assumption 4 and rearranging to isolate α gives

$$\alpha = -\frac{\Psi + R_g \int_P^{\text{LID}} T_e \, d \ln P}{R_g \int_p^{\text{LID}} \hat{T} \, d \ln P}. \quad (10)$$

Likewise, isolating α in Eq. (7) gives

$$\alpha = \frac{T_b - T_{be}}{\int_P^{\text{LID}} W\hat{T} \, d \ln P}. \quad (11)$$

Equating the right-hand sides of Eq. (10) and (11) and rearranging gives

$$T_b = T_{be} + A(\Psi + B), \quad (12)$$

where

$$A = -\frac{\int_P^{\text{LID}} W\hat{T} \, d \ln P}{R_g \int_P^{\text{LID}} \hat{T} \, d \ln P} \quad \text{and} \quad (13)$$

$$B = R_g \int_P^{\text{LID}} T_e d \ln P. \quad (14)$$

Equation (12) relates the brightness temperature in a storm to the geopotential thickness at the same point and the surrounding environmental temperature. It is only in the interpretation of A that the assumption of a constant anomaly profile becomes pertinent. Equations (12) and (13) are valid without that assumption, however, in that case A is not a constant. Making the reasonable assumption of a fixed shape for the anomaly profile results in a constant value for A and a linear relationship between brightness temperature and thickness.

Using Eq. (12) to express the difference in two ''nearby'' points in a storm, both referenced to the same environmental point external to the storm, shows that a locally differenced brightness temperature is proportional to the locally differenced change in geopotential thickness, that is,

$$\Delta T_b = A\Delta\Psi = Ag\Delta z. \quad (15)$$

Going back now to the gradient wind equation [Eq. (5)], and using Eq. (15) to replace the geopotential thickness, we have

$$V_g = -\frac{fR}{2} + \sqrt{\frac{f^2R^2}{4} + \frac{R}{A}\frac{dT_b}{dn}}. \quad (16)$$

It is Eqs. (15) and (16) that support the observed relationship between brightness temperature gradients and gradient level wind speeds. Following Kidder et al. (1980) we assume gradient level winds are related to surface winds via a simple linear scale factor. Also, the maximum sustained winds ($V_{\max}$) are usually observed on the right side of a moving cyclone where the large-scale wind flow adds to the cyclone-scale circulation. Since Eq. (16) applies to only the cyclone-scale component of $V_{\max}$, we will subtract the storm movement from National Hurricane Center (NHC) estimates of $V_{\max}$ for the purposes of comparing to the AMSU measurements. It might not be possible to determine the storm motion component of $V_{\max}$ from AMSU data since, for synoptic to planetary flow features, an upper boundary condition of zero flow will generally not exist in the stratosphere (Hirschberg and Fritsch 1993).

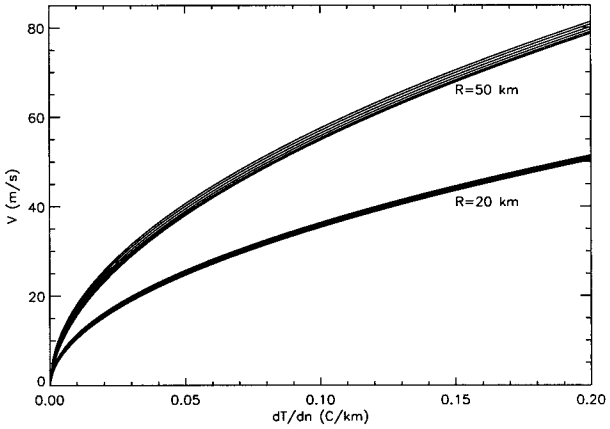

FIG. 2. Lower-tropospheric wind speeds computed from a modified version of the gradient wind equation [Eq. (16)] for two very different radii of curvature of the flow. For each radius several latitudes ranging from 1° to 50° were assumed.

Two important characteristics of Eq. (16) are the dependence of wind speed on the square root of the temperature gradient, and on the radius of curvature of the flow. This is illustrated in Fig. 2, where the sensitivity of temperature gradient to wind speed is displayed for two very different radii of curvature (20 km and 50 km), and at different latitudes (Coriolis parameters, f). Note that there is little dependence of the gradient wind speed on f.

There is, however, significant dependence on the radius of maximum sustained winds. This dependence might be difficult to address with AMSU data due to insufficient spatial resolution. The rest of our analysis depends upon the existence of a strong empirical relationship between the T_b gradients measured on the spatial scale that AMSU can measure (50 km at best), and those that exist on a smaller scale [on the order of 10 km; see Hawkins and Imbembo (1976)].

The marked nonlinearity of the relationship in Fig. 2 has important implications for unambiguously identifying and diagnosing the maximum sustained wind speed of tropical cyclones. Because there is little temperature change associated with wind speed changes at the lower wind speeds, depressions ($V_{\max} < 17$ m s^{-1}) and possibly tropical storms (17 m s^{-1} $< V_{\max} <$ 34 m s^{-1}) might be difficult to quantify with much accuracy

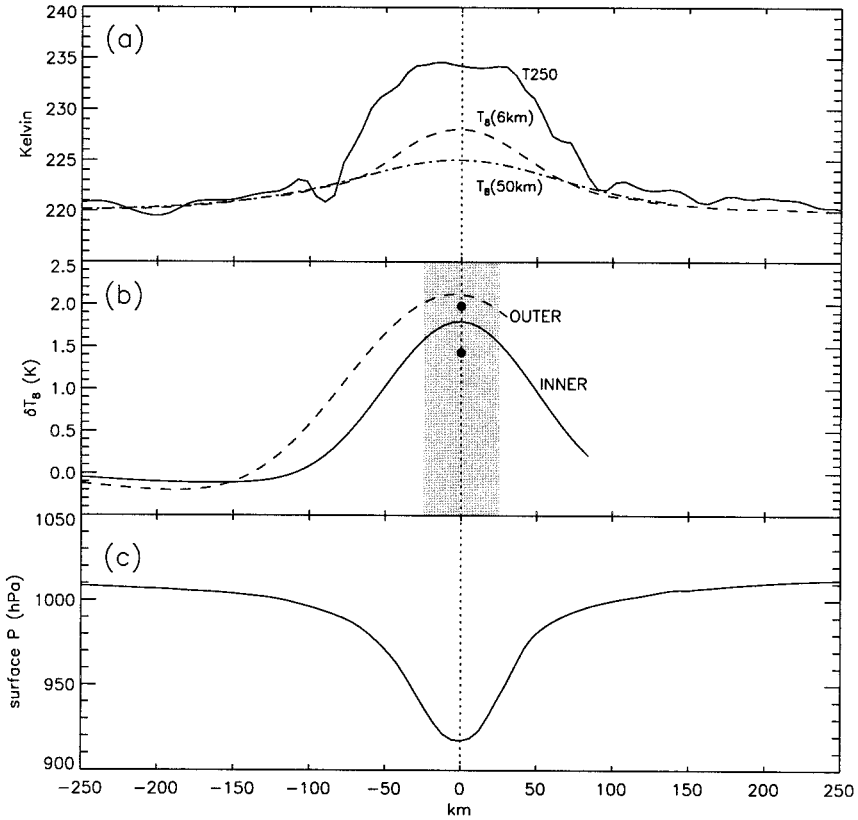

FIG. 3. East–west slice through Hurricane Andrew (1992) from mesoscale model simulations of (a) 250-hPa temperature, AMSU T_{b8} computed at the full model spatial resolution (6 km) and near the true AMSU resolution (50 km); (b) radially averaged T_b gradients for AMSU channel 8 for the ''inner'' and ''outer'' grids (see text for details); and (c) the surface pressure profile, which was used to define the warm core center location in the model simulation.

in the presence of measurement noise. While spatial averaging of the AMSU-A data can reduce noise, improving the situation somewhat, it also reduces the warm signal presented by the cyclone core. Fortunately, it can also be seen from Fig. 2 that increasing wind speeds are associated with nonlinearly increasing temperature gradients. Therefore, we might expect that satellite classification of tropical cyclone winds could be more accurate for hurricanes ($V_{\max} > 34$ m s^{-1}), and still more accurate for the more intense categories of hurricane. Theoretical evidence for this is presented next.

b. Mesoscale model simulations of Andrew (1992)

Another way of testing the theoretical relationship between near-surface winds and tropospheric temperature gradients is with mesoscale model simulations of a hurricane. We obtained Pennsylvania State University–National Center for Atmospheric Research fifth-generation Mesoscale Model simulated fields of Hurricane Andrew (Liu et al. 1997) spanning a 24-h period just before landfall. We computed AMSU brightness temperatures with a radiative transfer code at the full (6 km) resolution of the simulated field. We then computed dT_b/dn on each side of the warm core on spatial scales of 100 km and related the maximum temperature gradient observed to the maximum gridpoint wind speed at 10-m elevation. The resulting relationship between wind speed and the simulated AMSU T_{b7} gradients had a correlation of 0.9 and a standard deviation of 1.3 m s^{-1} over the wind speed range of 65–74 m s^{-1} for a sample size of 16 simulation times. This suggests that even small fluctuations in $V_{\max}$ have associated fluctuations in middle- and upper-tropospheric gradients in temperature, at least for the relative constant radius of curvature of the flow in Andrew during this time.

To illustrate the effect of AMSU sampling of Andrew's warm core, we computed T_{b8} at the full (6 km) model resolution, and also at the AMSU resolution, utilizing a two-dimensional Bessel function–based approximation of the AMSU antenna pattern with a half-power beamwidth of 50 km. The resulting magnitude of Andrew's warm core in AMSU channel 8 (Fig. 3a) is seen to be about one-half of that at the model's 250-hPa level. This reduction is due to the vertical averaging implicit in the channel 8 weighting function (see the appendix) combined with substantial sensitivity to the lower stratosphere, where the cyclone-scale temperature

perturbation disappears. At 50-km resolution, horizontal averaging further reduces the warm core intensity to about one-third of its magnitude at the 250-hPa level. Thus, the horizontal and vertical averaging of the AMSU measurements reduces a warm core of 15°C magnitude at 250 hPa to about 5°C in AMSU channel 8. We will return below to the Andrew simulations in the context of AMSU measurements of T_b gradients.

4. AMSU data analysis

While the previous section outlined a theoretical framework for understanding why upper-tropospheric data from microwave temperature sounders have sensitivity to near-surface wind speeds, there are at least two reasons why it is difficult to apply the theory directly to AMSU data. The existence of T_b depressions in the temperature channel data due to scattering from large ice particles in deep convection contaminates the warm core signal in those channels. This sensitivity to large ice was not realized in previous studies of tropical cyclones, as it was believed that the passive microwave signature of large ice particles was small. It has since been determined that these hydrometeors, through backscattering of upwelling radiation and virtually no reemission of radiation, can cause large T_b depressions, especially in microwave window channels. Localized T_b depressions as large as 200°C have been observed in the 85.5-GHz channel of the Special Sensor Microwave/Imager. The scattering effect was first reported in aircraft data (92 GHz) by Wilheit et al. (1982), and in satellite data (37 GHz) by Spencer et al. (1983), and it provides the basis for the estimation of convective rainfall by a number of investigators (e.g., Smith et. al. 1998)

The various temperature and hydrometeor effects can be seen in AMSU imagery (Fig. 4) of Hurricane Mitch near its peak intensity. The hurricane warm core is seen most clearly in the upper-tropospheric channels (6–9). The 220-K contour of channel 8 is shown in all images, and it represents the approximate size of the AMSU footprint at this scan angle (about 60 km). The reported eye diameter near this time was 35 km. The window and lower-tropospheric temperature channels, in contrast, indicate a range of sensitivities to liquid and ice hydrometeors. Over the ocean, channels 1 (23.8 GHz) and 2 (31.4 GHz) are primarily sensitive to rain and cloud water, which produce a warm signal against the radiometrically cold (low emissivity) background. Progressing from channel 3 (50.3 GHz) to channel 5 (53.596 GHz), we see a gradual loss of sensitivity to liquid hydrometeors, due to rising weighting functions having less weight below the freezing level (see the appendix, Fig. A1), while scattering due to large ice is increasingly evident in the form of local depression in the T_b. Note that one must go up to channel 7 (peaking at 250 hPa) before most of the visual evidence of ice hydrometeor contamination is lost. This suggests that adjustments for hydrometeor effects will be required to fully exploit the warm core signal in the AMSU channels.

The second reason for difficulty in applying the theory directly to AMSU data is that the AMSU spatial resolution (50 km at best) and sampling geometry is not sufficient to resolve the sharp temperature gradients that exist above the peak surface wind speeds, which occur on scales on the order of 10 km (e.g., Andrew; Fig. 3). As mentioned above, the success of AMSU for monitoring $V_{\max}$ will depend upon a strong empirical relationship between the temperature gradients measured by AMSU (50-km scale, at best) and the gradients that exist above the region of maximum sustained winds (on the order of 10 km). A related issue is the inability of the AMSU spatial resolution to resolve variations in the radius of curvature (radial location) of the maximum sustained winds.

a. Variables and case selection

Because of these hydrometeor and spatial resolution considerations, we have developed our algorithm based upon empirical analysis of AMSU-A data, but with variables guided by our theoretical analysis. The theory outlined above suggests that T_b gradient variables, and the square of those variables, should capture most of the functional dependence of Eq. (16). Figure 2 suggests that variations in the Coriolis force can be neglected. Because of the hydrometeor effects, we have included all AMSU channels that are most sensitive to hydrometeors (channels 1–4, and 15), as well as the temperature channels (5–10), in our regression experiments. The inclusion of hydrometeor information will, in effect, allow an empirical ''hydrometeor correction'' to the temperature channels to statistically optimize the regression match to NHC estimates of $V_{\max}$.

The spatial sampling of the AMSU instrument illustrated in Fig. 1 includes the general case of a tropical cyclone warm core positioned somewhere in the swath. It can be seen that the spatial resolution (footprint size nominally 50 km) of the measurements degrades away from nadir, especially in the cross-track direction. The sampling interval also degrades in the cross-track direction, but it does not change in the alongtrack direction. Although it would be possible to use gridded AMSU data, we have chosen to utilize only the individual footprint measurements in our technique.

While the spatial resolution of the AMSU data is typically larger than the cyclone eye diameter, this does not necessarily mean that we should restrict our analysis to only those measurements nearest the warm core. While the highest-resolution gradient information will maximize the warm core signal, it will also have higher noise than a larger-scale estimate that includes an average of more footprints. Therefore, we included in our analysis AMSU variables computed at two spatial resolutions. The first is a radially averaged T_b gradient ($\delta_r T_b$) at an ''inner grid'' resolution [$\delta_r T_{b(\text{inner})}$] estimated

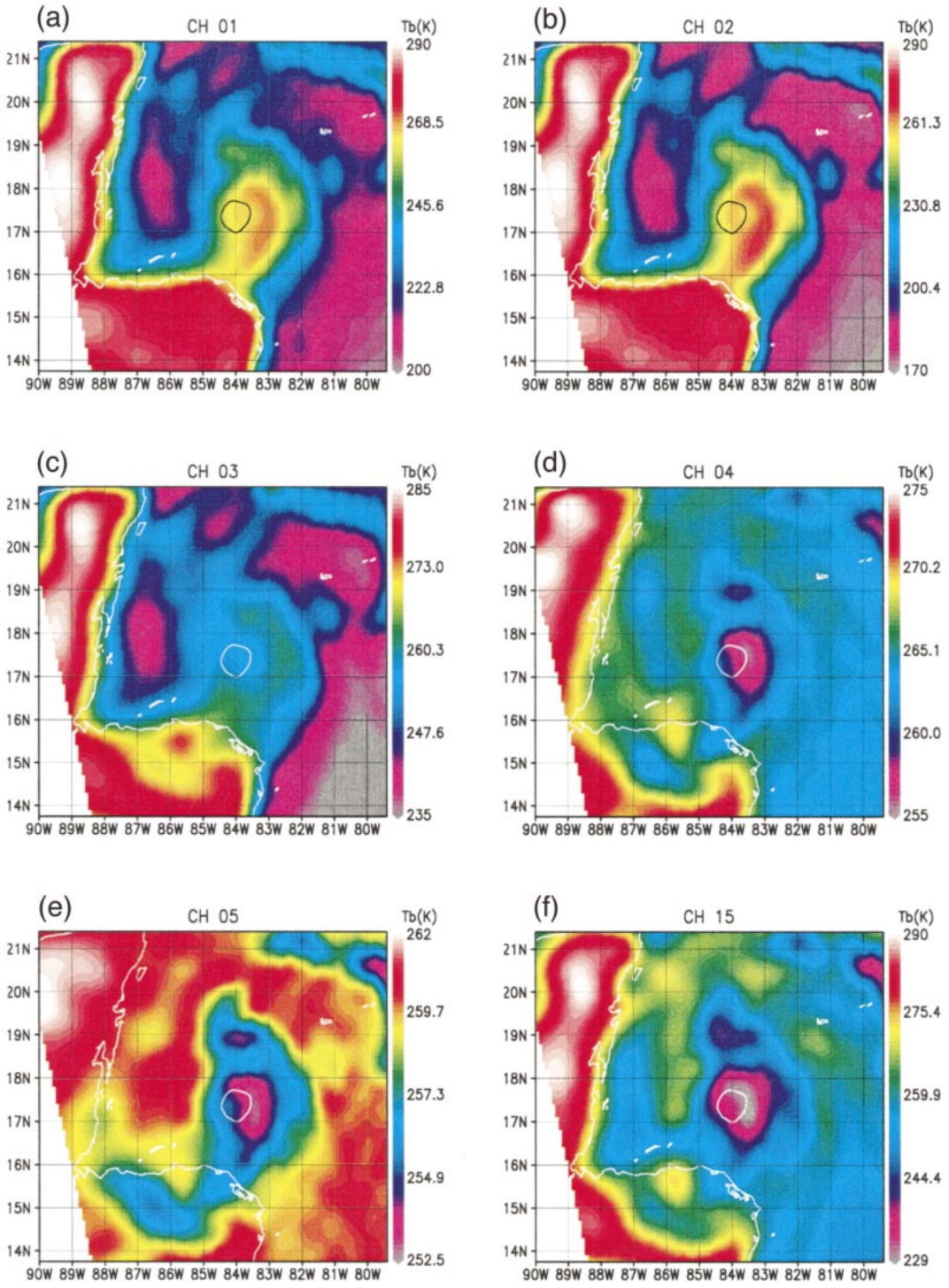

FIG. 4. Hurricane Mitch imagery from AMSU channels 1–9 and 15 when Mitch was north of Honduras (0040 UTC 27 Oct 1998). (a)–(f) Hydrometeor-sensitive channels (1–5, 15). (g)–(j) channels primarily sensitive to the hurricane warm core (6–9). The original resolution (50 km) of the AMSU imagery has been interpolated to about 10-km resolution based upon an optimum interpolation method (Poe 1990) that utilizes an approximation of the AMSU antenna pattern.

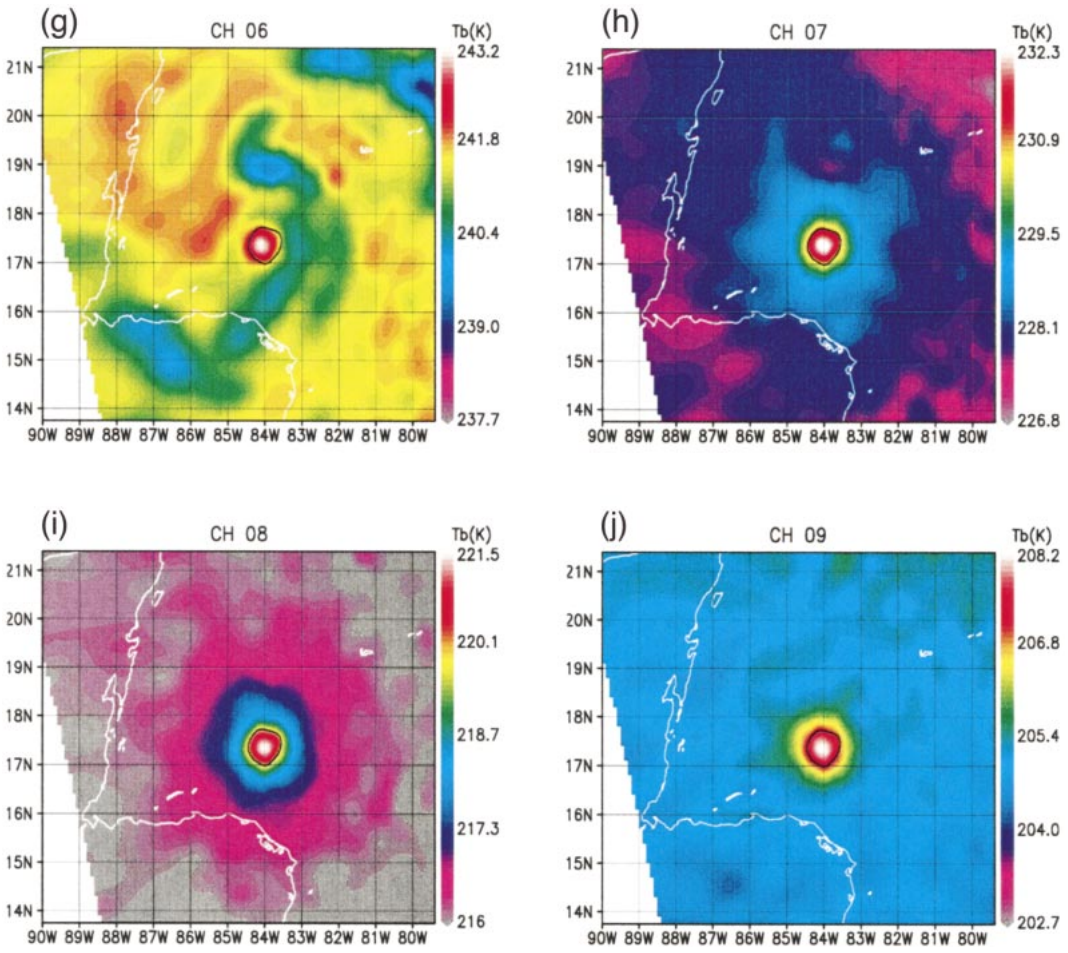

FIG. 4. (*Continued*) A white or black circle indicates the 220-K contour of the warm core in channel 8 and also represents the approximate size of the AMSU footprint (about 60 km) at this position in the swath. The reported eye diameter at this time was 35 km.

as the difference between the center footprint T_b with the average of the surrounding eight footprints T_b (see Fig. 1). The second is an ''outer grid'' resolution $\delta_r T_b$ estimated with a T_b average over the inner 3×3 contiguous footprints minus the average T_b of the immediately surrounding 16 footprints (also in Fig. 1). Computed in this fashion, $\delta_r T_{b(\text{outer})}$ has a noise value of 0.06°C for channels 7 or 8, while the inner grid gradient has about 0.15°C noise. The resulting gradients correspond to average distances of about 65 km at nadir for the inner region, and somewhat more than that for the outer region. Now returning to the Andrew simulations, calculations of $\delta_r T_{b8(\text{inner})}$ and $\delta_r T_{b8(\text{outer})}$ result in gradients of 1.5°–2°C magnitude, respectively, when Andrew had 70 m s^{-1} peak winds (Fig. 3b). Note that these AMSU-simulated gradients for Andrew (equivalent to about 0.03°C km^{-1}) are only 10% of the temperature gradient at 250 hPa (0.31°C km^{-1}), due to vertical and horizontal averaging inherent in the AMSU measurements. Furthermore, we see that $\delta_r T_{b8(\text{inner})}$ is smaller than $\delta_r T_{b8(\text{outer})}$, probably due to the rather wide (50 km) warm core of Andrew at this time. Also shown in Fig. 3b are the corresponding average AMSU gradients from four observations of Mitch (1998) and one of Lenny (1999), having maximum wind speeds of 64–74 m s^{-1}. These measurements are in reasonable agreement with the model simulations of Andrew at about the same intensity, except that the Mitch and Lenny averages have $\delta_r T_{b8(\text{inner})}$ larger than $\delta_r T_{b8(\text{ourter})}$, possible due to smaller warm cores in those storms.

The effect of the AMSU measurements not being centered on the cyclone warm core can also be deduced from Fig. 3b. The shaded region represents a range of AMSU alignments with the center of the warm core, from AMSU exactly aligned with the warm core center (the center of the shaded region) to the warm core center falling exactly between two AMSU footprints (the edge of the shaded region). It can be seen that such misalignment effects result in a $\pm 5\%$ variation in the AMSU diagnoses of radially averaged T_b gradients for Andrew.

Gradients in an ice scattering index were also computed. The scattering index (SI_{89}) is a measure of the

TABLE 2. Atlantic tropical cyclones that were sampled by AMSU after 3 Aug 1998, and their range of NHC-reported maximum sustained wind speeds. The wind speeds have the storm motion subtracted and are interpolated to the satellite observation time. Storms located over land or poleward of 40°N were excluded form the analysis, as were warm cores sampled by AMSU footprints 1–3 or 28–30 (out of 30).

Storm	No. of cases	Min storm-relative V_{max} (m s^{-1})	Max storm-relative V_{max} (m s^{-1})
Bonnie	7	5	46
Charley	2	13	19
Danielle	11	5	42
Earl	4	14	19
Frances	3	12	16
Georges	14	7	47
Hermine	5	11	19
Ivan	6	9	31
Jeanne	15	11	41
Karl	9	8	35
Lisa	5	13	20
Mitch	12	7	74
Nicole	11	9	30
Arlene	6	9	24
Bret	5	15	45
Cindy	14	9	46
Dennis	8	13	40
Emily	2	13	16
Floyd	7	20	52
Gert	14	15	60
Harvey	3	19	21
Irene	6	25	29
Jose	7	16	25
Katrina	5	6	15
Lenny	9	9	64

degree to which the 89-GHz (channel 15) T_b's are depressed below the theoretically expected T_b for an oceanic atmosphere that matches the observed channel 1 (23.8 GHz) and 2 (31.4 GHz) measurements (Grody et al. 2000). Those authors report that values of SI_{89} that exceed 7°C suggest ice scattering influence on channel 15. We also included the square of all of these gradient terms in an attempt to capture the nonlinear character of Eq. (16). Finally, we included area-averaged T_b terms for channels 1–10, and SI_{89}, for the inner region in case there was additional information that was not contained in the gradient terms.

All of these statistics were compiled for those cyclone cases in the final NHC archive of Atlantic cyclones from the 1998 and 1999 hurricane seasons. We matched AMSU data to the NHC archived cyclone locations within certain space and time bounds. The NHC reported cyclone position and V_{max} at 6-hourly resolution were interpolated to the satellite observation time. When the interpolated position fell within the AMSU swath and its interpolated time was within 3 h of the AMSU observation time, we found the warmest AMSU footprint within two footprints of the interpolated NHC cyclone position. The AMSU location of the warm core was defined as the footprint having a local maximum in $\delta_r T_{b8(\text{outer})}$. For this location, the values of $\delta_r T_{bi}$ over the inner and outer grids were computed for channels 1–10 and channel 15 SI, and stored along with the inner grid average T_b for further analysis.

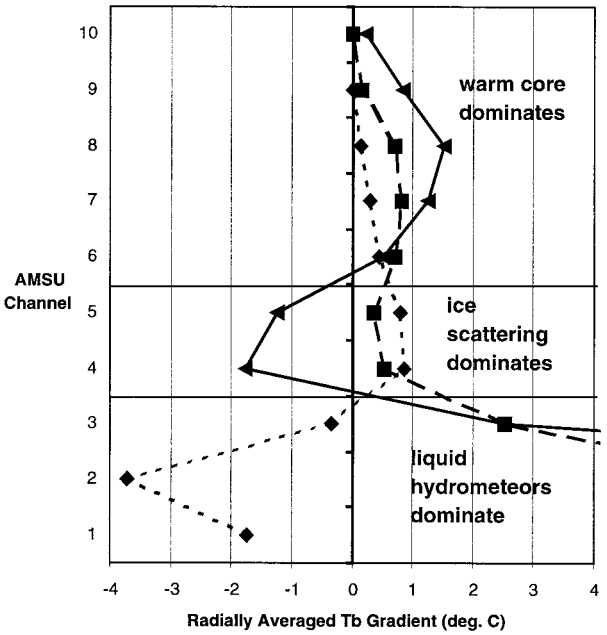

FIG. 5. "Vertical" profiles of average $\delta_r T_{b8\ (\text{outer})}$ for three classes of tropical cyclone intensity: 10–30 m s^{-1} (42 cases, dotted), 30–50 m s^{-1} (31 cases, dashed), and >50 m s^{-1} (9 cases, solid).

The NHC-reported locations bounding the AMSU observation were also used to compute the speed of storm motion, which was then subtracted from V_{max} to get a storm-relative wind speed. It is significant that various regression analysis experiments verified that correlations were substantially higher with the storm movement removed from V_{max}. This is consistent with the theoretical expectation that cyclone-scale AMSU gradients do not contain information on the large-scale flow component of V_{max}. Neglect of this effect might have reduced the apparent skill in previous studies that estimated V_{max} with MSU data. It also requires that operational application of this method to AMSU data will need an estimate of cyclone speed of motion to add to the storm-relative V_{max} estimate.

Cyclones over land were excluded, as were those that listed by NHC as "extratropical," and any storms poleward of 40°N. This procedure generated 190 storm matchups for 25 cyclones (listed in Table 2).

b. Average $\delta_r T_b$ profiles

We examined the average $\delta_r T_b$ characteristics for three categories of NHC V_{max} for the 82 cases that had in situ observations (primarily aircraft reconnaissance, RECON; Fig. 5). These categories were less than 30 m s^{-1}, greater than 30 m s^{-1} but less than 50 m s^{-1}, and greater than 50 m s^{-1}. The profiles reveal increasing warming of the upper-tropospheric channels (7–9) as

TABLE 3. Regression results from the NHC V_{max} vs AMSU variable stepwise regression analysis for 82 RECON cases during the 1998 and 1999 Atlantic hurricane seasons. Shown with each regression coefficient is the ordering of term selection by their contribution to the regression fit. The regression constant is 12.27 m s^{-1}, and the explained variance is 93%.

Channel no.	Primary sensitivities	$\delta_r T_{b(\text{inner})}$	$[\delta_r T_{b(\text{inner})}]^2$	$\delta_r T_{b(\text{outer})}$	$[\delta_r T_{b(\text{outer})}]^2$	Avg T_b	(Avg T_b)^2
1	Hydrometeors, water vapor						
2	Hydrometeors						
3	Hydrometeors, T (950 hPa)						
4	T (900 hPa), hydrometeors		6 (0.20155)				
5	T (600 hPa), hydrometeors						
6	T (400 hPa)						
7	T (250 hPa)				2 (−3.02546)		
8	T (150 hPa)		5 (2.55445)	1 (52.706)	3 (−16.04306)		
9	T (90 hPa)						
10	T (50 hPa)						
SI	Hydrometeors	4 (0.1704)					

cyclone intensity increases. The negative gradients that form in the middle-tropospheric channels (4, 5) for the stronger categories of cyclone are the result of scattering by large ice near the warm core overwhelming the warm core signal. This interpretation is supported by the δSI_{89} averages as well, which reveal negligible gradients in ice scattering for the weakest systems ($\delta SI_{89} = -4.4$°C) and moderate systems ($\delta SI_{89} = 4.2$°C), but much more ice scattering near the warm core for the intense systems ($\delta SI_{89} = 16.1$°C). Finally, the large positive and negative gradients in channels 1–3 are due to cloud and rainwater contamination dominating the inner and outer averaging areas, respectively, depending upon cyclone intensity.

c. Regression results

The linear and nonlinear terms in Table 3 were provided to the stepwise regression procedure and are assumed to capture most of the functional dependence inherent in Eq. (16). Consistent with the small dependence of Eq. (16) on the Coriolis parameter (Fig. 2), regression terms that included it did not add any improvement in test regressions, and so were excluded from the analysis.

The regression results for the 82 RECON cases are contained in Table 3. The regression step number and regression coefficients are listed for those terms deemed to be statistically significant at the 98% confidence level. The explained variance is 93.3% and the standard deviation of the regression error is 3.9 m s^{-1}. A more independent measure of the regression performance was estimated by a series of 82 jackknifed regressions (e.g., Elsner and Schmertmann 1994), leaving one case out in each for independent testing. The average standard deviation of the errors and explained variance from that set of regressions was 4.7 m s^{-1} and 93.4%, respectively, compared to 3.9 m s^{-1} and 93.3% without jackknifing. As might be expected for the AMSU instrument's new capabilities, these levels of skill are better than previous studies with MSU data [e.g., 6.7 m s^{-1}; Velden (1989)]. The $\delta_r T_{b8(\text{outer})}$ term provided the most information on V_{max}, while $[\delta_r T_{b7(\text{outer})}]^2$, $[\delta_r T_{b8(\text{outer})}]^2$, and $[\delta_r T_{b8(\text{inner})}]^2$ were chosen as well for their warm core information. The other two of the six terms chosen by the regression, $\delta SI_{89(\text{inner})}$ and $[\delta_r T_{b4(\text{inner})}]^2$, are hydrometeor sensitive and likely provide hydrometeor corrections to the other regression terms. Consistent with Eq. (16), note that none of the area-averaged T_b terms were chosen by the regression. Only the gradient terms were needed to explain variations in storm-relative maximum sustained wind speeds.

The high level of agreement (4.7 m s^{-1}) is somewhat surprising in light of the dependence of V_{max} of the radius of curvature of the flow (which, in turn, would be related to the eye diameter) shown in Fig. 2. We speculate that the inclusion of gradient information at two spatial scales could be providing some empirical information on the size of the eye. Merrill (1995) addressed the use of certain constraints in attempting to match poorer spatial resolution MSU data to hurricane eyes with smaller spatial scales.

The regression skill for the 108 cases that had no in situ measurements of surface winds (NO-RECON, Table 4) is considerably poorer than the skill for the 82 RECON cases, with an explained variance of 63% and an error standard deviation of 7.2 m s^{-1}. Jackknifed regressions had an error standard deviation of 7.5 m s^{-1}. The only two terms chosen, $\delta_r T_{b8(\text{outer})}$ and $[\delta_r T_{b7(\text{outer})}]^2$, are the same as the first two chosen in the RECON regression. No other terms were found to add significant additional information. The source of the NO-RECON winds was presumably entirely due to Dvorak (1984) estimates from Geostationary Operational Environmental Satellite data.

A scatter diagram of the NHC versus AMSU regression diagnoses of V_{max} for the 82 RECON cases (Fig. 6) reveals no appreciable degradation as wind speeds increase. The corresponding scatter diagram for the 108 NO-RECON cases (Fig. 7) illustrates the poorer agreement when no in situ surface wind measurements are available. There is some hint that the discrepancy between the RECON and NO-RECON skills is restricted

TABLE 4. As in Table 3 except for 108 NO-RECON cases. The regression constant is 11.2 m s^{-1}, and the explained variance is 63%.

Channel no.	Primary sensitivities	$\delta_r T_{b(\text{inner})}$	$[\delta_r T_{b(\text{inner})}]^2$	$\delta_r T_{b(\text{outer})}$	$[\delta_r T_{b(\text{outer})}]^2$	Avg T_b	(Avg T_b)^2
1	Hydrometeors, water vapor						
2	Hydrometeors						
3	Hydrometeors, T (950 hPa)						
4	T (900 hPa), hydrometeors						
5	T (600 hPa), hydrometeors						
6	T (400 hPa)						
7	T (250 hPa)				2 (−13.7713)		
8	T (150 hPa)			1 (49.720)			
9	T (90 hPa)						
10	T (50 hPa)						
SI	Hydrometeors						

to $V_{\max}$ below about 45 m s^{-1}. Since the RECON estimates are presumably more accurate than Dvorak (NO-RECON) estimates, the jackknifed regression result for the comparisons to RECON (4.7 m s^{-1}) is probably a better indication of the AMSU accuracy than is the NO-RECON regression result (7.5 m s^{-1}).

It is not known what, if any, biases might exist in the application of the Atlantic storm–trained equation to other ocean basins. It is likely that changes in boundary layer stability related to local sea surface temperature conditions will require adjustments to the AMSU-diagnosed winds, since the AMSU vertical resolution probably cannot resolve such details, especially in the presence of substantial hydrometeor contamination.

5. Operational implementation considerations

We have implemented the described procedure for the automated identification of tropical cyclones using the regression equation detailed in Table 3. To address false alarm reduction, the resulting tropical cyclone diagnoses were made for the global tropical oceans and compared to events reported by various operational forecasting centers. We found that a low false alarm rate requires setting the detection threshold fairly high (minimal tropical storm strength, 17 m s^{-1}). This is partly because, as discussed above, the temperature signal of weak tropical cyclones is very small. But it is also related to the relative rarity of tropical cyclones in the AMSU database. If we assume that the warm core of a tropical cyclone will influence only a few AMSU measurements on any given day, this amounts to less than 0.01% of all tropical measurements. Thus, even though the AMSU 1σ measurement noise value of $\delta_r T_{b8(\text{outer})}$ is low (0.06°C), a very small percentage of the data will have much larger noise values, resulting in occasional false alarms. In addition, some of the false alarms are due to extratropical vorticity maxima that have some of the same characteristics in the AMSU data as do tropical warm core systems (Velden 1992; Spencer et al. 1995). Another, although infrequent, source of false alarms is bad data.

Removal of most false alarms was accomplished by requiring that any warm core diagnoses of at least trop-

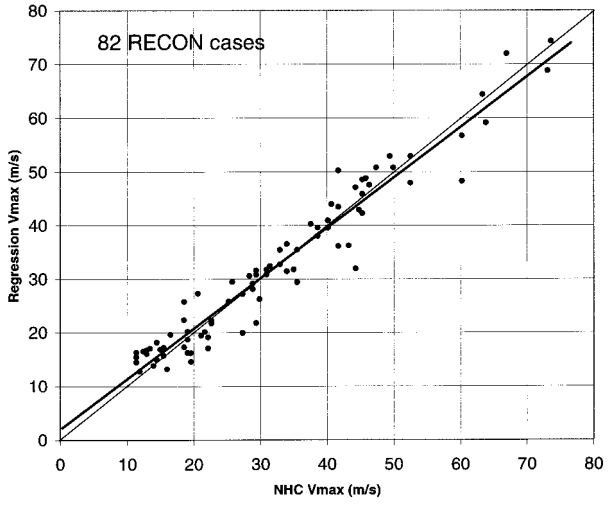

FIG. 6. Regression-equation (Table 3) estimates vs NHC estimates of $V_{\max}$ for 82 RECON cases during the 1998 and 199 hurricane seasons. The explained variance is 93%.

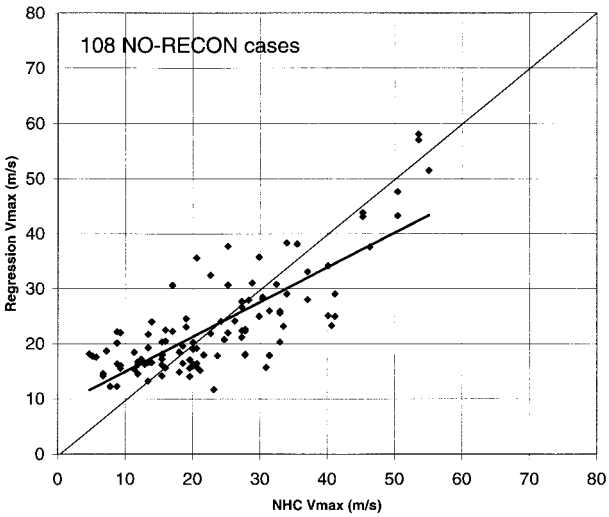

FIG. 7. As in Fig. 6 except for 108 NO-RECON cases. The explained variance is 63%.

ical storm strength also met several other criteria. A potential warm core was identified if any T_{b8} was at least 0.12°C warmer than all of the immediately surrounding eight footprints. Furthermore, for at least one footprint in the 5×5 grid of footprints centered on the warm core footprint, 1) the maximum value of SI_{89} had to be at least 20°C, indicating the presence of deep convection; 2) maximum total integrated water vapor, computed according to Grody et al. (2000), must exceed 55 mm, indicating the presence of tropical air; 3) minimum total integrated water vapor must not be less than 40 mm, indicating a lack of very dry extratropical air; and 4) the average of these maximum and minimum vapor values must be least 60 mm. An obvious alternative to AMSU-only diagnosis of tropical cyclones would be the inclusion of other data, such as visible and infrared satellite imagery, but such an enhancement was beyond the scope of this study. While AMSU estimates could be restricted to only the known positions of tropical cyclones, we wanted to explore the feasibility of identifying tropical cyclones based upon temperature sounder data alone.

6. Summary and conclusions

Building upon previous work, an updated theoretical basis has been described to explain the observed close relationship between localized upper-tropospheric warming and surface wind speeds in tropical cyclones. This treatment shows that, with appropriate assumptions, warm core cyclone-scale height gradients in the lower troposphere (and thus wind speeds) are nonlinearly related to radially averaged gradients in middle- and upper-tropospheric T_b measurements from microwave temperature sounders. The theoretical analysis depends upon the existence of an upper boundary condition of no cyclone-scale height variations in the stratosphere. This boundary condition is necessary in order to translate T_b gradients (which are quasi-thickness gradients) into lower- to middle-tropospheric height gradients.

Because of hydrometeor contamination of the lower- and middle-tropospheric sounding channels, as well as the inability of the AMSU to resolve the finescale of horizontal temperature gradients above the region of maximum sustained winds, it is difficult to apply the theory directly to AMSU data. AMSU imagery of Mitch (1998) illustrated the contaminating influence of ice hydrometeors on the temperature sounding channels. Mesoscale model simulations of Andrew (1992) reveal the extent to which the AMSU sampling degrades the warm core signal. Therefore, we used the theory as a guide to select satellite-measured parameters that were then empirically related to NHC estimates of maximum sustained wind speed (V_{max}) through stepwise regression. This empirical calibration of the method necessarily assumes that the NHC estimates of V_{max} are unbiased; hence, the current method cannot be utilized to determine whether biases in NHC estimates of V_{max} exist.

For the 1998 and 1999 Atlantic hurricane seasons, 82 space–time matches were made between AMSU and NHC reports of tropical cyclones when in situ wind estimates were available (RECON), while 108 cases had no in situ wind measurements (NO-RECON). The NHC estimates of V_{max} in the latter cases were dominated by the Dvorak method. The resulting skill of the regressions was markedly different between the RECON and NO-RECON sets of data. For 82 cases that had in situ measurements of V_{max}, the jackknifed regression error standard deviation was 4.7 m s^{-1}, while for the 108 cases without in situ wind data, the error standard deviation was 7.5 m s^{-1}. Presumably the RECON-based estimates are more accurate than the Dvorak-based estimates, and so the lower (4.7 m s^{-1}) figure is probably more representative of the AMSU skill, at least for the Atlantic cyclones addressed in this study. While the T_b gradient calculations restrict the potentially usable AMSU swath to footprint positions 3–28 (out of 30), we restricted it further to footprint positions 4–27 as we noticed a significant reduction in skill when prints 3 and 28 were included in the regressions.

Implementation the RECON-based regression algorithm required several screening tests to reduce the number of false alarms. These included not only the identification of a warm core of at least tropical storm strength, but screening for sufficient total integrated water vapor and the presence of deep convective ice signatures in the 89-GHz channel. (The near-real time estimates are available on the Wide World Web at http://pm-esip.msfc.nasa.gov/cyclone.)

It is not known whether the method developed here will provide unbiased estimates in other ocean basins. Probably the largest uncertainty is the coupling of the mid- to lower-tropospheric circulation (that the AMSU method infers) to the surface. We speculate that AMSU estimates will be too high over anomalously cool water, and too low over anomalously warm water, compared to the cyclones used for training in this study (West Atlantic, Caribbean, and Gulf of Mexico). Another limitation of the method is a lack of information on variations in the radius of curvature of the maximum sustained winds in different storms. Nevertheless, the high level of agreement we find between RECON and AMSU measurements suggests this might not be a major source of error. It might well be that the T_b gradient information contained in our variables at two spatial resolutions includes some empirical information on the eye diameter, but this is merely speculative. Finally, additional AMSUs to be launched on NOAA-L, -M, -N, -N′, NASA's Aqua satellite, and the Météorologie Opérationelle satellite will provide additional sources of data for monitoring of tropical cyclones.

Acknowledgments. This research was sponsored by NASA's Earth Science Information Partner program and

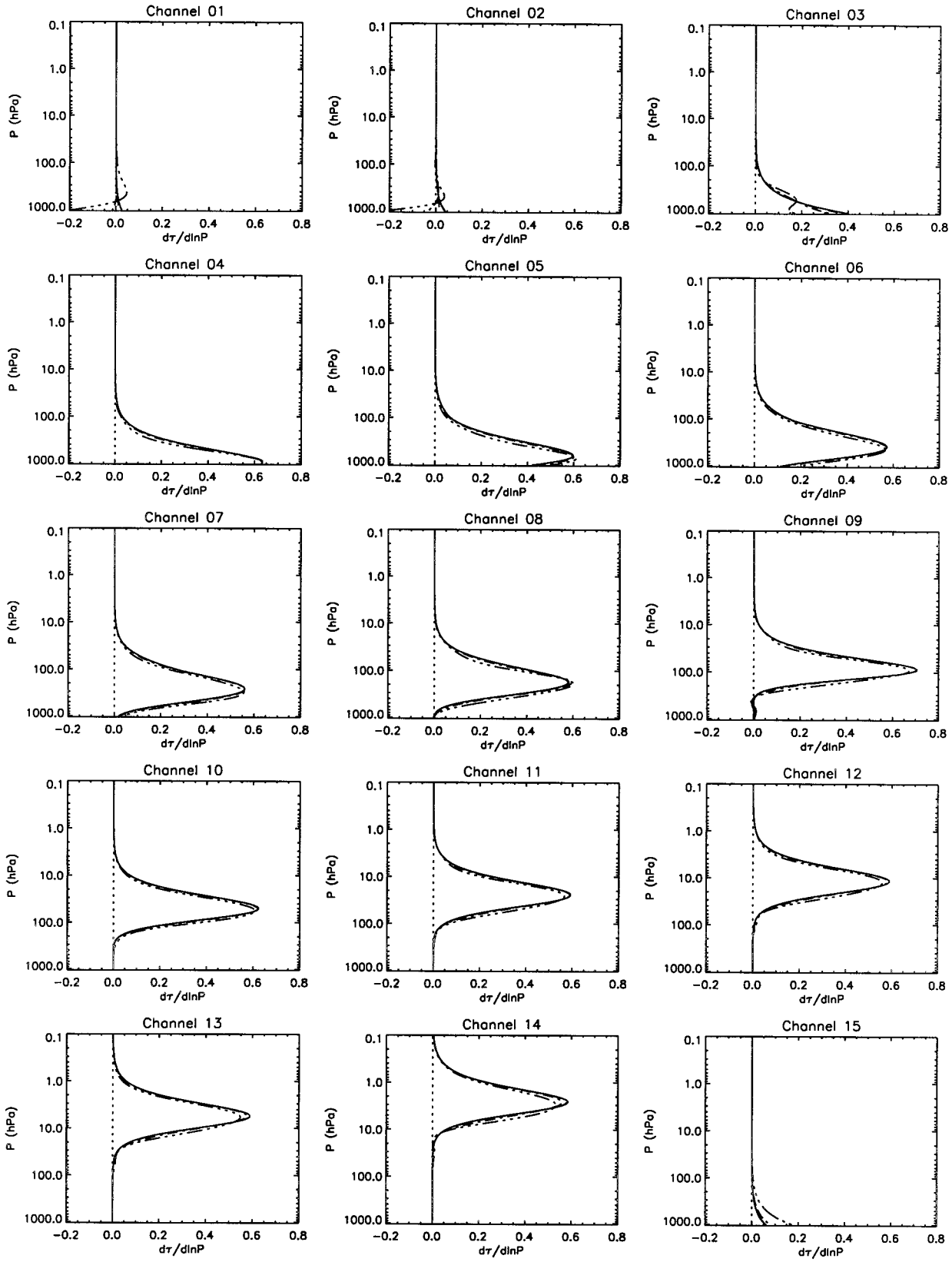

FIG. A1. AMSU-A nadir-weighting functions (solid) and limb correction averaging kernels (dotted–dashed) for earth incidence angles of 17.0° (footprint positions 11 and 20); 36.38° (6 and 25), and 57.58° (1 and 30). Due to the goodness of fit, only the extreme angle (57.58°) can be seen in all panels.

NASA's Earth Science Enterprise. We thank Chris Landsea, Chris Velden, and an anonymous reviewer for helpful suggestions regarding improvement of the manuscript.

APPENDIX

Limb Correction of AMSU Data

As a through-nadir scanning temperature sounder scans away from nadir, the increased pathlength of the radiation through the atmosphere causes the weighting function to rise in altitude, causing the familiar limb-darkening effect. We developed limb-correction equations for all of the AMSU channels to compute limb-corrected T_b at any non-nadir beam position with a linear combination of a subset of the AMSU channels that have sensitivity to the layer in question. Since the AMSU does not have a nadir beam position, all of the view angles other than 15 (1–14; see Fig. 1 in the text) are corrected to view angle position 15 (the nearest position to nadir). We utilized multiple linear regression analysis on a set of T_b's calculated from 1761 radiosonde soundings in the global Television Infrared Observational Satellite (TIROS) Operational Vertical Sounder (TOVS) Initial Guess Retrieval (TIGR) database (Chedin et al. 1985) to find the best fit, in a least squares sense, between the position 15 T_b for a given channel and several channels T_b at the other view angles,

$$T_{bk}^{*} = c_0 + \sum_{i=1}^{15} c_{k,i} T_{bb} + c_e.$$

The limb-corrected T_b for channel $k(T_{bk}^{*})$ is then a linear combination of the $i = 1$, 15 channels of AMSU (see Table 1 in the text). This is applied separately for each footprint position using only channels from that footprint. Separate regression equations were developed for land (assumed emissivity = 0.95) and ocean [emissivity ranging between 0.4 and 0.6, based upon Klein and Swift (1977)]. Only those channels having weighting functions that significantly overlap the desired nadir weighting function were employed, so that the unused channels' coefficients in Eq. (1) are set to zero. While the regression coefficients are then based upon radiative transfer theory, ''striping'' in limb-corrected T_b imagery suggested the need for additional empirical offsets (c_e). These were computed for each of the 30 beam positions, every 10 days, in 10° latitude bands, land and ocean separately. In application of the limb correction procedure to AMSU data, a ⅙° percentage of water coverage database was utilized to compute the relative proportions of land versus ocean limb correction equations and empirical offsets to be averaged together.

The resulting fits of the limb correction averaging kernels at view angle positions 1, 6, and 11 to the position 15 weighting functions are shown in Fig. A1. It can be seen that very close fits are obtained.

An alternative procedure involving least squares matching of weighting functions, rather than T_b, was also tested. For those channels having very small sensitivity to the surface, the resulting limb correction equation coefficients were nearly identical to those based upon T_b matching. This alternative procedure was abandoned, however, because the surface influence on several of the channels could not be easily accounted for.

FORTRAN code for the application of the limb correction procedure is available from the corresponding author.

REFERENCES

Chedin, A., N. A. Scott, C. Wahiche, and P. Moulinier, 1985: The improved initialization inversion method: A high resolution physical method for temperature retrievals from satellites of the TIROS-N series. *J. Climate Appl. Meteor.*, **24,** 128–143.

Dvorak, V. F., 1984: Tropical cyclone intensity analysis using satellite data. NOAA Tech. Rep. NESDIS 11, NOAA, U.S. Department of Commerce.

Elsner, J. B., and C. P. Schmertmann, 1994: Assessing forecast skill through cross validation. *Wea. Forecasting*, **9,** 619–624.

Franklin, J. L., M. L. Black, and K. Valde, 2000: Eyewall wind profiles in hurricanes determined by GPS dropwindsondes. Preprints, *24th Conf. on Hurricane and Tropical Meteorology*, Fort Lauderdale, FL, Amer. Meteor. Soc., 446–447.

Grody, N. C., C. M. Hayden, C. C. Shen, P. W. Rosenkranz, and D. H. Staelin, 1979: Typhoon June winds estimated from scanning microwave spectrometer measurements at 55.45 GHz. *J. Geophys. Res.*, **84,** 3689–3695.

——, F. Weng, and R. Ferraro, 2000: Application of AMSU for obtaining hydrological parameters, *Microwave Radiometry and Remote Sensing of the Earth's Surface and Atmosphere*, P. Pampaloni and S. Paloscia, Eds., VSP, 339–351.

Hawkins, H. F., and S. M. Imbembo, 1976: The structure of a small, intense hurricane—Inez 1966. *Mon. Wea. Rev.*, **104,** 419–442.

Hirschberg, P. A., and A. M. Fritsch, 1993: On understanding height tendency. *Mon. Wea. Rev.*, **121,** 2646–2661.

Jarvinen, B. R., C. J. Neumann, and M. A. S. Davis, 1984: A tropical cyclone data tape for the North Atlantic Basin, 1886–1983. NOAA Tech. Memo. NWS NHC 22, 21 pp.

Kidder, S. Q., W. M. Gray, and T. H. VonderHaar, 1978: Estimating tropical cyclone central pressure and outer winds from satellite microwave data. *Mon. Wea. Rev.*, **106,** 1458–1464.

——, ——, and ——, 1980: Tropical cyclone surface winds derived from satellite microwave sounder data. *Mon. Wea. Rev.*, **108,** 144–152.

Klein, J. A., and C. T. Swift, 1977: An improved model for the dielectric constant of sea water at microwave frequencies. *IEEE J. Oceanic Eng.*, **OE-2,** 104–111.

Liu, Y., D.-L. Zhang, and M. K. Yau, 1997: A multiscale numerical study of Hurricane Andrew (1992). Part I: Explicit simulation and verification. *Mon. Wea. Rev.*, **125,** 3073–3093.

Merrill, R. T., 1995: Simulations of physical retrieval of tropical cyclone thermal structure using 55-GHz band passive microwave observations from polar-orbiting satellites. *J. Appl. Meteor.*, **34,** 773–787.

Mo, T., 1996: Prelaunch calibration of the Advanced Microwave Sounding Unit-A for NOAA-K. *IEEE Trans. Microwave Theory Techniques*, **44,** 1460–1469.

Nunez, E., and W. M. Gray, 1977: A comparison between West Indies hurricanes and Pacific typhoons. Postprints, *11th Tech. Conf. on Hurricanes and Tropical Meteorology*, Miami, FL, Amer. Meteor. Soc., 528–534.

Poe, G. A., 1990: Optimum interpolation of imaging microwave radiometer data. *IEEE Trans. Geosci. Remote Sensing*, **GE-28,** 800–810.

Smith, E. A., and Coauthors, 1998: Results of the WetNet PIP-2 project. *J. Atmos. Sci.,* **55,** 1483–1536.

Spencer, R. W., W. S. Olson, W. Rongzhang, D. W. Martin, J. A. Weinman, and D. A. Santek, 1983: Heavy thunderstorms observed over land by the Nimbus-7 Scanning Multichannel Microwave Radiometer. *J. Climate Appl. Meteor.,* **22,** 1041–1046.

——, W. M. Lapenta, and F. R. Robertson, 1995: Vorticity and vertical motions diagnosed from satellite deep layer temperatures. *Mon. Wea. Rev.,* **123,** 1800–1810.

Velden, C. S., 1989: Observational analyses of North Atlantic tropical cyclones from NOAA polar-orbiting satellite microwave data. *J. Appl. Meteor.,* **28,** 59–70.

——, 1992: Satellite-based microwave observations of tropopause-level thermal anomalies: Qualitative applications in extratropical cyclone events. *Wea. Forecasting,* **7,** 669–682.

——, and W. L. Smith, 1983: Monitoring tropical cyclone evolution with NOAA satellite microwave observations. *J. Climate Appl. Meteor.,* **22,** 714–724.

——, B. M. Goodman, and R. T. Merrill, 1991: Western North Pacific tropical cyclone intensity estimation from NOAA polar-orbiting satellite microwave data. *Mon. Wea. Rev.,* **119,** 159–168.

Wilheit, T. T., and Coauthors, 1982: Microwave radiometric observation near 19.35, 92, and 183 GHz of precipitation in Tropical Storm Cora. *J. Appl. Meteor.,* **21,** 1137–1145.